DOI: 10.1002/ejic.201100312

Revisiting the Zintl–Klemm Concept: A_2AuBi (A = Li or Na)

Fei Wang[a] and Gordon J. Miller*[a]

Dedicated to Professor John D. Corbett on the occasion of his 85th birthday

Keywords: Solid-state structures / Diamond network / Zintl phases / Zintl–Klemm formalism / Gold / Bismuth / Thallium / Alkali metals / Electronic structure / Density functional calculations

Alkali metal gold bismuthides, A_2AuBi, are isoelectronic with alkali metal thallides, ATl = A_2TlTl, and yet Na_2AuBi adopts an orthorhombic structure with a 1-D zigzag "ribbon" structural motif rather than the cubic double diamond structure type of NaTl as well as Li_2AuBi. Using first principles quantum mechanical calculations applied to A_2AuBi, hypothetical "A_2HgPb," and A_2TlTl, and comprehensively decomposing the total energies into metallicity, ionicity, and covalency components to establish parallels with the qualitative Zintl–Klemm formalism, the factors determining the relative stability between the zigzag "ribbon" and the diamond network are examined. An interplay between volume-dependent energy terms, i.e., metallicity or ionicity, and covalency among the electronegative components determines which structural motif is favored. In Na_2AuBi, there are two factors stabilizing the zigzag "ribbon." Au 5*d* states significantly interact with Bi 6*p* states, especially Au $5d_{x^2-y^2}$ with Bi $6p_z$ to promote stronger Au–Bi covalent interactions than in the diamond network. This factor does not exist in Na_2TlTl and "A_2HgPb," where Hg, Tl, and Pb 5*d* states are well localized. Secondly, the zigzag ribbons provide effective covalent interactions at larger volumes, as in Na_2AuBi, while effective covalent interactions occur in the diamond network only at smaller volume, as in Li_2AuBi.

Introduction

The Zintl–Klemm concept, though simple, can effectively rationalize the structures of Zintl phases and polar intermetallic compounds.[1–8] The essence and originality of the Zintl–Klemm concept are the inclusion of both charge transfer and covalent interactions into the structural rationalization of compounds, many of which are composed of metallic elements. For instance, to rationalize the so-called double diamond structure of NaTl,[9] the Zintl–Klemm concept claims that, after obtaining one valence electron from each Na atom, each resulting Tl^- "anion" with four valence electrons will follow the octet rule and form four "covalent" bonds with neighboring Tl^-. This positive success of the Zintl–Klemm concept implies that it is justifiable and beneficial to consider charge transfer and covalent interactions in intermetallic compounds.

However, the simplicity of the Zintl–Klemm concept also causes its limitations. In another report, we addressed the structures of alkali metal trielides including LiTl, NaTl, KTl,[10] in which the formal "Tl^-" does not behave precisely like a tetrel atom. The electronic structure of NaTl revealed that the Tl 6*s* orbitals are virtually filled, so these electrons are like lone pairs. Therefore, unlike the tetrel atoms in a diamond-type network, the formal "Tl^-" does not involve sp^3 hybridization. Also, although most alkali metal trielides adopt the double diamond structure, LiTl adopts the CsCl-type structure, and KTl features $[Tl_6]^{6-}$ octahedra. Neither of these two structural exceptions can be understood from this simple formalism. We demonstrated that to rationalize the structures of Zintl phases, the interplay among long-range ionic, short-range covalent, and volume-dependent metallic interactions must be comprehensively considered in these intermetallic and metal-metalloid systems. By addressing the cases that defy the Zintl–Klemm rationalization, we are attempting to refine the Zintl–Klemm concept and deepen our understanding of the structures of Zintl phases.

Herein, we continue this effort by studying the (alkali metal)-gold-bismuth compounds, A_2AuBi (A = Li or Na). The recently synthesized, orthorhombic Na_2AuBi[11] imposes another challenge for the Zintl–Klemm concept. Its crystal structure is shown in Figure 1. Au and Bi atoms form one-dimensional zigzag "ribbons" along the *c*-axis. These ribbons consist of linear chains of Au atoms, bridged by Bi atoms on alternating sides. A similar structural motif is also observed in the isoelectronic gold monohalides.[12–14] Within the $[AuBi]^{2-}$ ribbon, the Au–Au and Au–Bi distances, respectively, are 2.924(1) Å and 2.752(1) Å. These

[a] Department of Chemistry, Iowa State University,
321 Spedding Hall, USA
Fax: +1-515-294-9623
E-mail: gmiller@iastate.edu

Supporting information for this article is available on the WWW under http://dx.doi.org/10.1002/ejic.201100312.

ribbons are juxtaposed in the *bc*-planes forming Au/Bi "sheets". The distance between Bi atoms from two neighboring ribbons is 4.216(1) Å, much larger than those within a ribbon, so these ribbons are well separated from one another. Na atoms reside between two neighboring Au/Bi sheets. Questions arise when we compare this structure with Li_2AuBi and NaTl, reformulated as Na_2TlTl, which both adopt the double diamond structure.

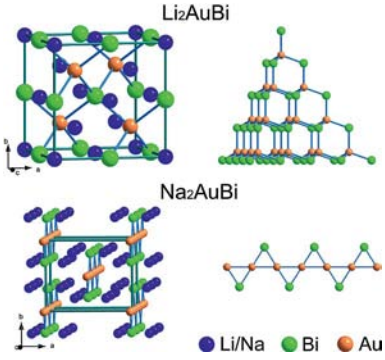

Figure 1. Crystal structures of Li_2AuBi and Na_2AuBi.

NaTl is isoelectronic with Na_2AuBi and, considering atomic number, Tl is the "average" of Au and Bi. From this point of view, it is justifiable to expect that Au/Bi and Tl atoms construct the same network, just like ZnSe[15] or GaAs[16] mimic the diamond structure of Ge. However, the Au/Bi zigzag ribbons in Na_2AuBi bear no resemblance with the Tl diamond network of NaTl.

On the other hand, in Li_2AuBi Au/Bi atoms do form the diamond network with only heteroatomic Au–Bi contacts (Figure 1).[17] The Zintl–Klemm formalism works well for this structure. By disregarding the 5*d* electrons of Au, and after gaining the 2*s* electrons from Li, the average valence electron count for each Au and Bi atom is 4 so, on average, each should form 4 "covalent bonds". If Au is considered as a one-electron donor as well, the valence electron count of Bi is 8, and there should be no Bi–Bi contacts. These two situations are satisfied in the diamond network with only heteroatomic Au–Bi contacts, but not in the zigzag ribbons, where each Au atom has contacts with two other Au atoms and two Bi atoms, and each Bi has two contacts with Au atoms. So, on average, each atom has three "bonds" in the ribbons. One possibility is that there is multiple bonding. Just like in graphite, although every C is bonded to only three neighbors, the delocalized π bond makes the fourth "bond" at each atom. Is this also the case in the Au/Bi ribbons? Or do they violate the octet rule so that the Zintl–Klemm concept does not apply to Na_2AuBi at all? In analogy with AuI,[14] each linear Bi–Au–Bi unit may involve 3-center, 4-electron bonds.[18] In this picture, since each Au–Bi interaction has bond order 1/2, then the 8-*N* rule places 7 valence electrons at each Bi atom, leading to a formulation $(Na^+)_2Au(Bi^{2-})$. On the other hand, since each Bi has two contacts with Au atoms, another formulation is viable, $(Na^+)_2Au^-(Bi^-)$. Therefore, given these various bonding scenarios, it is worthy to investigate how these zigzag ribbons are stabilized and why switching from Na to Li and from Au/Bi to Tl both render the structure to transform from orthorhombic with zigzag ribbons to the cubic double diamond structure.

Computational Methods

Model Structures

To answer the questions raised above, we built both orthorhombic and cubic model structures for first-principle calculations with the following compositions, Li_2AuBi, Na_2AuBi, and NaTl (Na_2TlTl). Moreover, we also built model structures for a hypothetical composition, "Na_2HgPb", which is considered as intermediate between Na_2AuBi and Na_2TlTl. The details of these model structures are listed in Table 1. The volume per formula unit, $V_{f.u.}$, in our calculations, is equal to either the experimental values or the equilibrium volumes obtained from the energy vs. volume, $E(V)$, curves calculated with VASP (details can be found in "VASP Calculations"). For the cubic model structures, $V_{f.u.}$ is the only variable. But, for the orthorhombic structures, there are also the atomic fractional coordinates (*x* and *y*) and the aspect ratios (*b*/*a* and *c*/*a*) of the unit cell to be determined. These were done by structural optimization with VASP. The obtained lattice parameters and atomic positions are reported in the section "Results and Discussions".

Table 1. Details of model structures.

Orthorhombic *Cm*cm				
Na/Li	8*g*	*x*	*y*	1/4
Au/Hg/Tl1	4*a*	1/2	1/2	0
Bi/Pb/Tl2	4*c*	1/2	*y*	1/4
Cubic *F*-43*m*				
Na/Li1	4*d*	3/4	3/4	3/4
Na/Li2	4*a*	0	0	0
Au/Hg/Tl1	4*c*	1/2	1/2	1/2
Bi/Pb/Tl2	4*b*	1/4	1/4	1/4

VASP Calcultions

We used the *Vienna* ab initio *simulation package* (VASP)[19–21] to optimize the orthorhombic structures and calculate the total energies, band structures, and valence electron density maps of the model structures. The projector augmented-wave (PAW)[22] pseudopotentials were adopted with the Perdew-Burke-Ernzerhof generalized gradient approximation (PBE-GGA),[23] in which scalar relativistic effects[24] are included. We did not consider spin-orbit coupling, which may well have an effect as revealed in our previous study on thallides.[25] We believe that such relativistic effects are not the determining factors here because the "ribbon"/"diamond" structural contrast also exists between Na_2AgSb[26] and NaIn,[27] where relativistic effects are much less significant. For structural optimization,

the conjugate gradient algorithm[28] was applied. The first Brillouin zone was sampled with a $5\times5\times5$ Monkhorst-Pack mesh.[29] The energy cutoffs are 242.9 eV for Na_2AuBi and Li_2AuBi, 237.8 eV for Na_2HgPb, and 237.1 eV for Na_2TlTl. For the calculations of total energies, band structures, and valence electron density maps, a denser $7\times7\times7$ Monkhorst-Pack mesh was used and the energy cutoffs were also higher: 303.6 eV for for Na_2AuBi and Li_2AuBi, 297.3 eV for Na_2HgPb, and 296.3 eV for Na_2TlTl. The valence electron density maps were plotted with *wxDragon*.[30]

We scanned total energies of the model structures over certain ranges of volumes to study their energy vs. volume behavior. The cubic model structures were isotropically expanded and compressed while, for the orthorhombic model structures, we optimized the atomic coordinates and the aspect ratios of unit cells at each sampling volume before the total energies are calculated. The obtained $E(V)$ curves were fitted to the Murnaghan equation of state,[31] from which the equilibrium volumes (V_{eq}) were determined. Total energies were then calculated at these V_{eq}. And again, structural optimization preceded the energy calculation for each orthorhombic model structure at V_{eq}.

All calculated total energies were partitioned into an electrostatic term (E_{ES}) and an electronic term ($E_{electronic}$). By comparing E_{ES} values of different structures, we can evaluate which structure is favored if the valence electrons are highly delocalized, as in classical metals. Comparison of $E_{electronic}$, on the other hand, evaluates the effects of valence electron localization, including charge transfer, formation of lone pairs, and covalent bonds. The details of this energy partitioning Scheme is included in our preceding reports.[10,25]

LMTO Calculations

The Stuttgart *Tight-Binding, Linear-Muffin-Tin Orbital* program with *Atomic Sphere Approximation* (TB-LMTO-ASA)[32] was utilized to calculate the density of states (DOS) and crystal orbital Hamiltonian population (COHP)[33] curves of the model structures. The integrated COHP (ICOHP) values were employed to evaluate the effect of covalent interactions. It quantifies the energy difference between the crystal orbitals and non-interacting atomic orbitals. In all calculations, the exchange and correlation energy was treated with the von Barth-Hedin local density approximation.[34] All relativistic effects except spin-orbit coupling were taken into account using a scalar relativistic approximation.[35] The basis sets include 2*s* and 2*p* for Li, 3*s* and 3*p* for Na, and 5*d*, 6*s*, and 6*p* for Au, Hg, Tl, Pb, and Bi. In some calculations, the 5*d* of Au, Hg, and Tl were excluded from basis sets. By comparing the results with and without these 5*d* orbitals, we evaluated their effects in covalent interactions. Reciprocal space integrations were performed with an $8\times8\times8$ k-points mesh. The unit cells of the model structures were filled with Wigner-Seitz spheres, the radii of which were adjusted so that the sums of the sphere volumes are equal to the volumes of the unit cells. Empty atomic spheres were generated by the program where they are necessary. The overall overlaps between atomic spheres in all model structures range from 8.07% to 9.59%.

Results and Discussion

Na_2AuBi, "Na_2HgPb", and Na_2TlTl

The experimental volumes per f.u. of Na_2AuBi and NaTl (Na_2TlTl) are very close, 106.35 and 103.22 Å^3/f.u. respectively. To explore their differences, we compared the cubic and orthorhombic structures at these two volumes for Na_2AuBi, Na_2TlTl, as well as the hypothetical, intermediate composition "Na_2HgPb".

The optimized orthorhombic structures of Na_2AuBi, "Na_2HgPb", and Na_2TlTl are tabulated in detail in Table 2 with selected interatomic distances listed in Table 3. Comparison between orthorhombic Na_2AuBi, optimized at 106.35 Å^3/f.u., and its experimental structure[11] shows that the structural optimization shortened *a* and *b* but elongated *c*. The optimized structure also has larger interatomic distances in the zigzag ribbons. But, overall, the differences

Table 2. Lattice parameters and atomic positions of the optimized orthorhombic Li_2AuBi, Na_2AuBi, "Na_2HgPb", and Na_2TlTl at various volumes. The experimental Na_2AuBi (exp.) is included for comparison.

			Li_2AuBi		Na_2AuBi				Na_2HgPb		Na_2TlTl	
V (Å^3/f.u.)			73.52	106.35	73.52	103.22	106.35	106.35 (exp.)	103.22	106.35	103.22	106.35
a (Å)			7.7183	9.1362	7.9482	9.2835	9.4253	9.447(2)	9.2649	9.3767	8.6713	8.8213
b (Å)			6.9904	8.1573	7.0148	7.5963	7.6511	7.700(2)	7.6194	7.6806	7.7969	7.8257
c (Å)			5.4505	5.7079	5.2744	5.8661	5.8989	5.849(1)	5.8491	5.9066	6.1071	6.1621
Na/Li	*8g*	*x*	0.1810	0.1711	0.1852	0.1815	0.1809	0.182(1)	0.1894	0.1887	0.1885	0.1885
		y	0.3032	0.2363	0.3196	0.3237	0.3235	0.333(1)	0.3207	0.3221	0.3154	0.3160
		z	1/4	1/4	1/4	1/4	1/4	1/4	1/4	1/4	1/4	1/4
Au/Hg/Tl1	*4a*	*x*	1/2	1/2	1/2	1/2	1/2	1/2	1/2	1/2	1/2	1/2
		y	1/2	1/2	1/2	1/2	1/2	1/2	1/2	1/2	1/2	1/2
		z	0	0	0	0	0	0	0	0	0	0
Bi/Pb/Tl2	*4c*	*x*	1/2	1/2	1/2	1/2	1/2	1/2	1/2	1/2	1/2	1/2
		y	0.1485	0.1956	0.1576	0.1847	0.1875	0.1973(1)	0.1548	0.1578	0.1355	0.1371
		z	1/4	1/4	1/4	1/4	1/4	1/4	1/4	1/4	1/4	1/4

Table 3. Selected interatomic distances (Å) of the optimized orthorhombic structures. d_{cubic} is the nearest neighbor distance in the cubic structure. All distances smaller than $2/3^{1/2}d_{cubic}$ (second nearest neighbor distance in the cubic structure) are listed.

		No./f.u.	73.52 Å^3/f.u. d_{cubic} = 2.880 Å		103.22 Å^3/f.u. d_{cubic} = 3.224 Å			106.35 Å^3/f.u. d_{cubic} = 3.257 Å				
			Li_2AuBi	Na_2AuBi	Na_2AuBi	Na_2HgPb	Na_2TlTl	Li_2AuBi	Na_2AuBi	Na_2AuBi (exp.)	Na_2HgPb	Na_2TlTl
Li/Na–	Li/Na	× 1	2.793	2.943	3.370	3.509	3.269	3.126	3.409	3.44(1)	3.539	3.325
		× 2	3.019	2.995	3.382	3.313	3.391	3.206	3.415	3.438(7)	3.357	3.426
	Au/Hg/Tl1	× 4	2.881	2.989	3.321	3.345	3.324	2.862	3.347	3.412(9)	3.381	3.355
		× 4	3.133	3.099	3.561	3.505	3.420	–	3.612	3.582(9)	3.545	3.464
	Bi/Pb/Tl2	× 2	2.689	2.748	3.139	3.092	2.983	3.024	3.182	3.18(1)	3.127	3.013
		× 2	2.789	2.790	3.219	3.143	3.044	–	3.266	3.29(1)	3.180	3.084
		× 4	3.081	3.024	3.378	3.416	3.485	3.301	3.408	3.400(5)	3.446	3.520
Au/Hg/Tl1–	Au/Hg/Tl1	× 1	2.725	2.637	2.928	2.925	3.054	2.854	2.949	2.924(1)	2.953	3.081
	Bi/Pb/Tl2	× 2	2.809	2.740	2.807	3.009	3.226	2.864	2.809	2.752(1)	3.015	3.231
Bi/Pb/Tl2–	Bi/Pb/Tl2	× 1	–	–	–	–	3.713	–	–	–	–	3.755

are small: those between experimental and optimized lattice parameters are all smaller than 0.05 Å, and all interatomic distances differ by less than 0.07 Å.

Replacing Au/Bi with Hg/Pb in the orthorhombic structure, at both volumes, alters the lattice parameters slightly, but the atomic position of Pb is significantly different from that of Bi. As a result, the Hg–Pb distances in the zigzag ribbons are over 0.2 Å larger than Au–Bi. As for the hypothetical orthorhombic Na_2TlTl, a is much smaller whereas b and c are much larger than for Na_2AuBi at the same volume. The interatomic distances in the Tl1/Tl2 zigzag ribbons are much larger than in the Au/Bi ribbons – Tl1–Tl1 is over 0.1 Å larger than Au–Au and Tl1–Tl2 is over 0.4 Å larger than the Au–Bi separation. Moreover, in Na_2AuBi, the distances between Bi exceed 4 Å, so the zigzag ribbons are "separated" from one another; but in Na_2TlTl, the corresponding Tl2···Tl2 distances are just over 3.7 Å, much shorter than Bi···Bi, so the Tl1/Tl2 zigzag ribbons tend to be "cross-linked" to each other.

In the double diamond structure, cubic symmetry requires uniform nearest neighbor interatomic distances, i.e., $d_{Na–Na} = d_{Na–Au/Hg/Tl1} = d_{Na–Bi/Pb/Tl2} = d_{Au/Hg/Tl1–Bi/Pb/Tl2}$ (in Table 3, these are all denoted by d_{cubic}). In the orthorhombic structure, however the distances can be different. According to Table 3, the interatomic distances in the zigzag Au/Bi ribbon of orthorhombic Na_2AuBi structure are much smaller than d_{cubic}, by ca. 0.30–0.45 Å, regardless of volume. This difference is much smaller in "Na_2HgPb" and Na_2TlTl, especially the latter, which is less than 0.18 Å.

Energy differences calculated using VASP between the orthorhombic and cubic structures are listed in Table 4 ($\Delta E = E_{ortho} - E_{cubic}$: $\Delta E < 0$ favors orthorhombic; $\Delta E > 0$ favors cubic); all agree with experiment. Orthorhombic Na_2AuBi and cubic Na_2TlTl each have the lower total energy (E_{TOT}). "Na_2HgPb" also favors the cubic structure, but by a smaller margin than in Na_2TlTl. Furthermore, the different volumes, 103.22 and 106.35 Å^3/f.u., do affect the magnitude but not the sign of ΔE_{TOT}. So, the structural difference between Na_2AuBi and Na_2TlTl is not caused by a volume effect. The electrostatic energy is always lower in the cubic structure, i.e., ΔE_{ES} is always positive for Na_2AuBi, "Na_2HgPb", and Na_2TlTl. This indicates that the cubic structure is favored over the orthorhombic structure by highly delocalized valence electrons or metallic interactions. On the other hand, the difference in electronic energy, $\Delta E_{electronic}$, is always negative. Therefore, valence electron localization stabilizes the orthorhombic structure more than the cubic structure. $\Delta E_{electronic}$ includes all effects from charge transfer, formation of lone pairs and covalent bonds, viz. the effects of ionicity and covalency are both involved. To evaluate the effects of ionic interactions, we have calculated the Madelung energy, $E_{Madelung}$, using the Ewald technique.[36] We then investigated the covalent interactions between the electronegative atoms (Au/Bi, Hg/Pb, and Tl1/Tl2) by calculating their ICOHP values using the LMTO method.

Table 4. Energy differences between the orthorhombic and cubic structures, $\Delta E = E_{ortho} - E_{cubic}$.

	Energy terms	73.52 Å^3/f.u.	103.22 Å^3/f.u.	106.35 Å^3/f.u.
Li_2AuBi	ΔE_{ES} [eV/f.u.]	–4.0443	–	102.1175
	$\Delta E_{electronic}$ [eV/f.u.]	4.2658		–102.6120
	ΔE_{TOT} [eV/f.u.]	0.2215		–0.4945
Na_2AuBi	ΔE_{ES} [eV/f.u.]	22.6768	90.8474	98.1157
	$\Delta E_{electronic}$ [eV/f.u.]	–21.9483	–91.1371	–98.4843
	ΔE_{TOT} [eV/f.u.]	0.7285	–0.2897	–0.3686
Na_2HgPb	ΔE_{ES} [eV/f.u.]	–	53.0567	58.0577
	$\Delta E_{electronic}$ [eV/f.u.]		–52.9061	–57.9580
	ΔE_{TOT} [eV/f.u.]		0.1506	0.0997
Na_2TlTl	ΔE_{ES} [eV/f.u.]	–	2.4928	7.5600
	$\Delta E_{electronic}$ [eV/f.u.]		–2.2125	–7.3193
	ΔE_{TOT} [eV/f.u.]		0.2803	0.2407

To calculate $E_{Madelung}$, Na is simplistically treated as Na^+, so that the (AuBi) substructure becomes $(AuBi)^{2–}$. Since one cannot precisely divide the two negative formal charges between Au and Bi, we calculated a range of formal charges from ($Au^{2–}Bi^0$) through ($Au^{–}Bi^{–}$) and ($Au^0Bi^{2–}$) to ($Au^+Bi^{3–}$). The difference in Madelung energies, $\Delta E_{Madelung}$, calculated all at 106.35 Å^3/f.u. relative to the cubic structure, is plotted against the formal charge on Au in Figure 2. The differences calculated at 103.22 Å^3/f.u. are close to these and included in Supporting Information. Apparently, the favoritism of ionicity toward the two structure types depends on how the two negative formal charges are assigned to Au and Bi. Between $Au^{–0.6}Bi^{–1.4}$ and $Au^{0.6}Bi^{–2.6}$,

$\Delta E_{Madelung}$ is negative and, beyond this range, positive. Considering their absolute electronegativities,[37] Au at 5.77 eV and Bi at 4.69 eV, we can estimate that Au should have more negative formal charges than Bi, or the formal charge of Au should be more negative than –1 [to the left of the (Au^-Bi^-) dotted line in Figure 2], which leads to positive $\Delta E_{Madelung}$ values according to Figure 2. So, ionicity favors the cubic structure for Na_2AuBi.

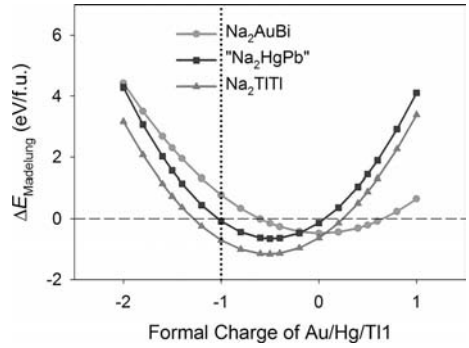

Figure 2. The difference in $E_{Madelung}$ between the two structure types calculated at 106.35 Å^3/f.u., $\Delta E_{Madelung} = E_{Madelung,ortho} - E_{Madelung,cubic}$, calculated at different formal charges on Au/Bi, Hg/Pb, Tl1/Tl2.

The same $\Delta E_{Madelung}$ curves are also plotted for "Na_2HgPb" and Na_2TlTl (Figure 2). The absolute electronegativities of Hg and Pb, respectively, are 4.91 eV and 3.9 eV.[37] So, the formal charge on Hg is expected to be more negative than on Pb (so, also left of the dotted line in Figure 2). Thus $\Delta E_{Madelung}$ is expected to be positive in "Na_2HgPb" as well; however, it is smaller (less positive) than in Na_2AuBi. Thus, for the hypothetical "Na_2HgPb", ionicity also favors the cubic structure. As for Na_2TlTl, it is Tl vs. Tl so it is reasonable to assign Tl^-Tl^-. $\Delta E_{Madelung}$ is negative according to Figure 2, so the orthorhombic structure is favored by ionicity.

The discussions above show that by evaluating energies associated with only metallicity or ionicity, we cannot yet successfully rationalize the relative stability between the zigzag ribbons and the diamond network in Na_2AuBi, "Na_2HgPb", and Na_2TlTl. At the same volume per f.u., metallicity always prefers the diamond network. Ionicity even contradicts with the observed structures – it prefers the cubic structure for Na_2AuBi, which adopts the orthorhombic structure, and prefers the orthorhombic structure in Na_2TlTl, which adopts the cubic structure.

To compare covalency between the two structure types, the differences in ICOHP, relative to those in the cubic structure, are also calculated at both 103.22 and 106.35 Å^3/f.u. for Na_2AuBi, "Na_2HgPb", and Na_2TlTl, and are listed in Table 5. It is evident that ΔICOHP shows exactly the same pattern with ΔE_{TOT} in Table 4. Na_2AuBi has negative ΔICOHP values at both volumes; "Na_2HgPb" and Na_2TlTl both have positive ΔICOHP values, which is smaller for "Na_2HgPb" than for Na_2TlTl. Therefore, although the zigzag ribbons do not follow the octet rule, its stability relative to the diamond network can still be rationalized with the Zintl–Klemm concept – the covalent interactions between the electronegative atoms determine the structure. In Na_2AuBi, the covalent interactions between Au/Bi atoms provide more stabilization by constructing the zigzag ribbon than the diamond network, so it prefers the former. The situations are exactly opposite in "Na_2HgPb" and Na_2TlTl – the covalent interactions between Hg/Pb atoms and between Tl1/Tl2 atoms stabilize the cubic structure more than the orthorhombic structure, rendering the diamond network more favorable.

Table 5. Difference in ICOHP values between the orthorhombic and the cubic structures (ΔICOHP = $ICOHP_{ortho} - ICOHP_{cubic}$) calculated with LMTO. The ΔICOHP values with subscript *sp* are calculated with the 5*d* orbitals of Au, Hg, and Tl1 excluded from basis set.

	ΔICOHP [eV/f.u.]	73.52 Å^3/f.u.	103.22 Å^3/f.u.	106.35 Å^3/f.u.
Li_2AuBi	$\Delta ICOHP_{Au/Bi}$	1.1132	–	–0.9022
	$\Delta ICOHP_{Au/Bi,sp}$	2.9131		0.2403
Na_2AuBi	$\Delta ICOHP_{Au/Bi}$	0.4466	–0.1469	–0.3324
	$\Delta ICOHP_{Au/Bi,sp}$	1.8806	0.9720	0.7972
Na_2HgPb	$\Delta ICOHP_{Hg/Pb}$	–	1.2052	1.0431
	$\Delta ICOHP_{Hg/Pb,sp}$		1.4939	1.3511
Na_2TlTl	$\Delta ICOHP_{Tl}$	–	1.8112	1.5779
	$\Delta ICOHP_{Tl,sp}$		1.8775	1.6398

To Figure out why the Au/Bi combination favors the zigzag ribbon but the isoelectronic Hg/Pb and Tl1/Tl2 combinations favor the diamond network, we studied the DOS and –COHP curves of Na_2AuBi, "Na_2HgPb", and Na_2TlTl. The curves calculated at 106.35 Å^3/f.u. are shown in Figure 3 and those calculated at 103.22 Å^3/f.u. are quite similar and included in Supporting Information.

For all cases, the majority of states below the Fermi levels are from Au/Bi, Hg/Pb, and Tl valence orbitals. Na also makes significant contributions, which implies that Na atoms do not donate all their 3*s* electrons to the electronegative counterparts. However, there is also an overestimation. For instance, in orthorhombic Na_2AuBi, the integrated DOS of Na at the Fermi level is 1.065 e^- per atom, making a formal $Na^{-0.065}$ anion. This is because LMTO evenly divides the "overlap population" when it calculates partial DOS and this results in overestimation for electropositive atoms and underestimation of electronegative atoms.[38]

The Fermi levels coincide with local minima or pseudogaps in all DOS curves as well as the bonding-antibonding crossovers in the Au–Bi, Hg–Pb, and Tl1–Tl2–COHP curves. Thus, although the zigzag ribbon does not satisfy the octet rule, it does provide optimized covalent interactions just like the diamond network. It is also evident that the Hg–Pb and Tl1–Tl2 interactions are weaker in the orthorhombic than in the cubic structure, but the Au–Bi interactions are comparable in both structures.

From the DOS curves, the most significant differences among Na_2AuBi, "Na_2HgPb", and Na_2TlTl are the relative positions of the 5*d*, 6*s*, and 6*p* states of Au/Bi, Hg/Pb, and Tl1/Tl2. To accentuate this feature, the population weighted band centers are shown in Figure 4. In the Tl1/Tl2 combi-

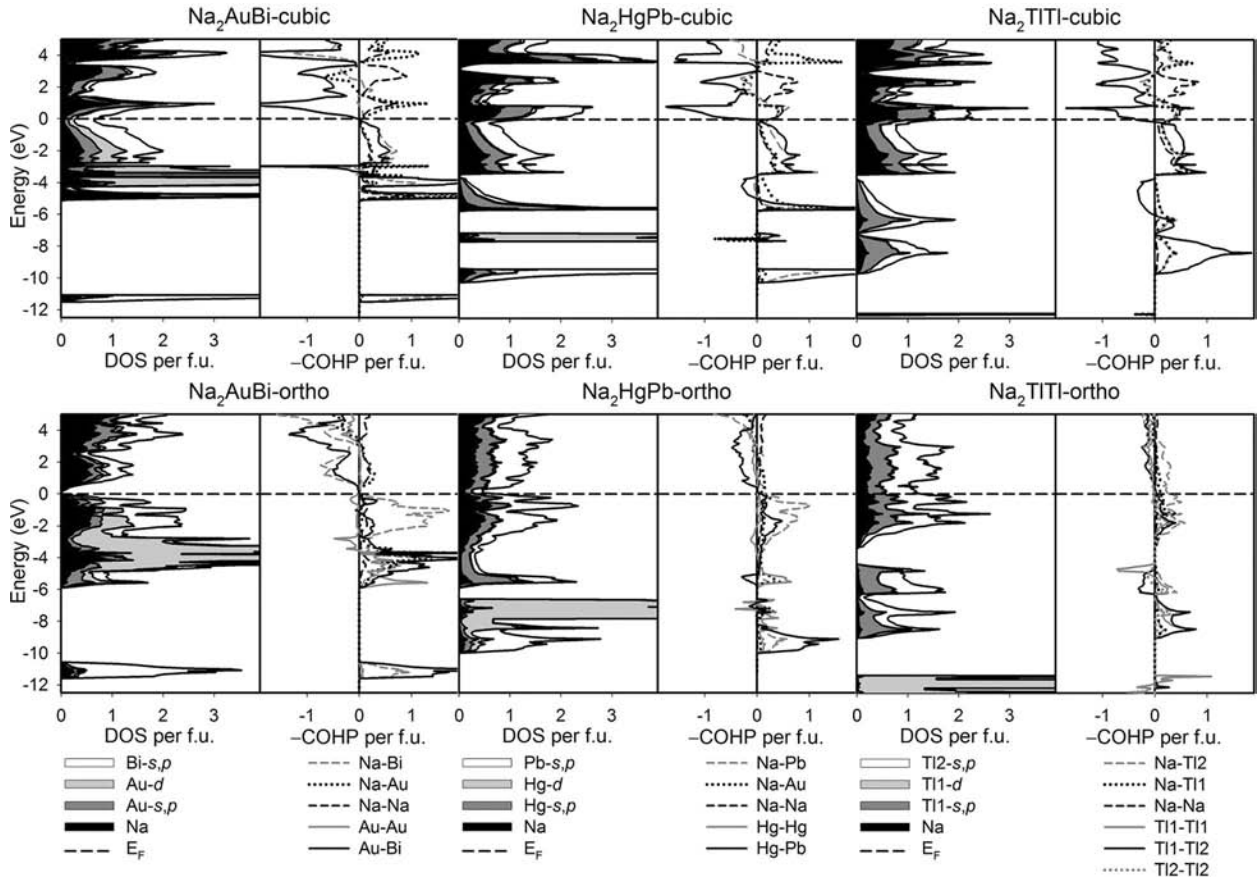

Figure 3. DOS and –COHP curves of Na_2AuBi, Na_2HgPb, and Na_2TlTl in both cubic and orthorhombic structures calculated with LMTO at 106.35 Å^3/f.u.

nation, the 5*d* states of Tl1 and Tl2 coincide and are localized around 12 eV below the Fermi level in the DOS curves. The –COHP curves demonstrate that these localized 5*d* states make no significant contributions to Tl–Tl covalent interactions. The band center of the Hg 5*d* states is just above that of Pb 6*s* states. The DOS curves reveal that Hg 5*d* states are also localized around –7.4 eV in the cubic structure and –7.2 eV in the orthorhombic structure, without perceivable contributions to those states just below the Fermi level (–6 to 0 eV). The –COHP curves also show that Hg 5*d* states have no significant contributions in Hg–Pb covalent interactions. In Au/Bi, the band center of Au 5*d* states is very close to the Bi 6*p* states, and only 3.5 eV below the Fermi level. The DOS curves tell that, in both structures, Au 5*d* states are among the states just below the Fermi level. And, the Au–Bi –COHP curves show these states to be bonding, although, in the cubic structure, there is an antibonding "spike" at –3 eV. Therefore, the difference between the isoelectronic Au/Bi, Hg/Pb, and Tl1/Tl2 combinations is that in Hg/Pb and Tl1/Tl2, 5*d* states are localized and do not significantly contribute to Hg–Pb and Tl–Tl covalent interactions, but, in Au/Bi, Au 5*d* states are actively involved in Au–Bi covalent interactions.

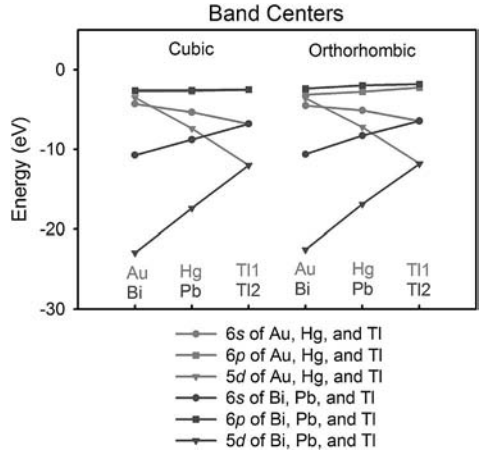

Figure 4. Population weighted band centers of the 5*d*, 6*s*, and 6*p* states of Au/Bi, Hg/Pb, and Tl1/Tl2.

To evaluate the effect of the 5*d* states of Au, Hg, and Tl1, we excluded them from the basis sets and re-calculated ICOHP values. These results are listed in Table 5 as $\Delta ICOHP_{sp}$. By excluding these 5*d* states, all ΔICOHP values increase, i.e., the orthorhombic structure becomes less favored. The largest increase occurs in Na_2AuBi and it is decisive – the sign of ΔICOHP changes from negative (favoring the orthorhombic structure) to positive (favoring the cubic structure). Therefore, the reason why the zigzag ribbon is only favored by Au/Bi is that Au 5*d* states stabilize it. Without the effective involvement of 5*d* states in covalent

interactions, as in Hg/Pb and Tl1/Tl2, the diamond network is preferred. This also explains why the zigzag ribbon defies the octet rule but still provides optimized covalent interactions – the octet rule applies when valence states consist of only *s* and *p* states.

To study how Au 5*d* states contribute to Au–Bi covalent interactions, we calculated the band structure of orthorhombic Na_2AuBi at 106.35 Å^3/f.u. and examined the eigenvectors of the bands at certain high symmetry *k*-points (Figure 5). The most significant interaction between Au 5*d* states and Bi orbitals is that between Au $5d_{x^2-y^2}$ and Bi $6p_z$. We located three bands at the *X* ($2\pi/a$, 0, 0), *Γ* (0, 0, 0), and *S* (π/a, $-\pi/b$, 0) points, where *a* and *b* are lattice parameters. They are indicated with arrows and sketched, along valence electron density maps calculated using VASP, in Figure 5 and their eigenvectors are included in Supporting Information. The dominant contributors of these bands exhibit bonding overlap between Au $5d_{x^2-y^2}$ and Bi $6p_z$ orbitals, such that the corresponding Au–Au interaction has δ* character along the ribbon.

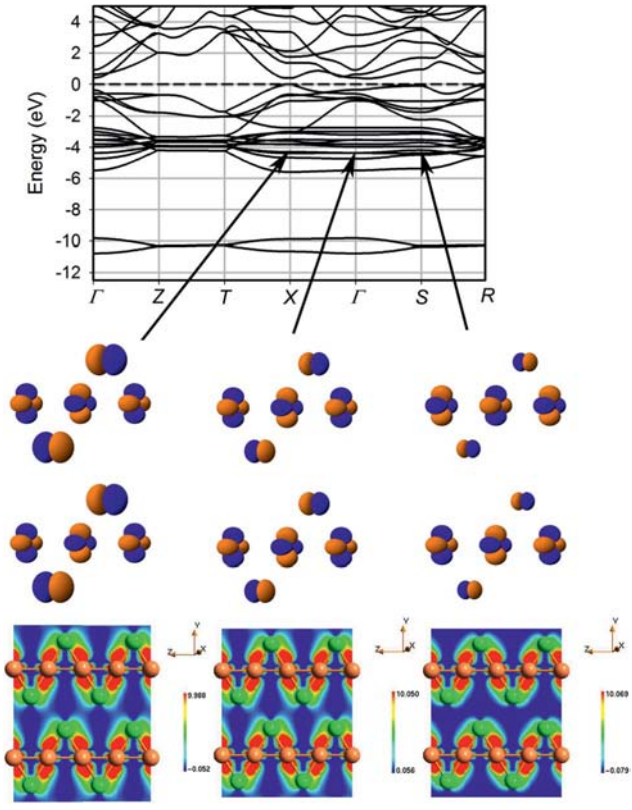

Figure 5. Band structure of orthorhombic Na_2AuBi at 106.35 Å^3/f.u. calculated with VASP and the sketches and valence electron density maps of the three bands demonstrating the interactions between Au $5d_{x^2-y^2}$ and Bi $6p_z$.

In conclusion, at the two volumes we studied, 103.22 and 106.35 Å^3/f.u., metallicity stabilizes the cubic structure more than the orthorhombic structure. Ionicity also favors the cubic structure in Na_2AuBi. Covalent interactions between electronegative atoms provide more stabilization in the zigzag ribbon for Au/Bi but, for Hg/Pb and Tl1/Tl2, it is the diamond network that provides more stabilization through covalency. The reason is that unlike Hg and Tl, Au 5*d* states are actively involved in covalent interactions. So Au/Bi is a 5*d*-6*s*-6*p* system and Hg/Pb and Tl1/Tl2 are essentially 6*s*-6*p* systems. While the diamond network satisfies the octet rule and is, thus, a good solution for an *s*-*p* system, the zigzag ribbon is a better solution for a *d*-*s*-*p* system because it provides effective bonding interactions between *d* and *sp* states, especially between Au $5d_{x^2-y^2}$ and Bi $6p_z$. And eventually, covalency prevails over metallicity and ionicity in Na_2AuBi, rendering it to adopt the orthorhombic structure.

Li_2AuBi and Na_2AuBi

The experimental volume of Li_2AuBi, 73.52 Å^3/f.u., is much smaller than that of Na_2AuBi, 106.35 Å^3/f.u. Therefore, we studied Li_2AuBi and Na_2AuBi in cubic and orthorhombic structures at both volumes. The optimized orthorhombic structures and selected interatomic distances are also listed in Table 2 and Table 3. Compared to orthorhombic Na_2AuBi, orthorhombic Li_2AuBi has smaller *a* values at both volumes. Since the *a* parameter determines the space between two neighboring "sheets" containing the Au/Bi zigzag ribbons, where the alkali metal atoms reside, it is closely related to the size of the alkali metal atoms. That Li is smaller than Na effects a smaller *a* parameter for Li_2AuBi than for Na_2AuBi. The dimension of the zigzag ribbons, however, is very close between orthorhombic Li_2AuBi and Na_2AuBi at both volumes – the differences in d_{Au-Au} and d_{Au-Bi} are all smaller than 0.1 Å. Moreover, the volume difference does not significantly affect the dimension of the zigzag ribbons, either. Through compression from 106.35 to 73.52 Å^3/f.u., d_{Au-Bi} shrinks by only 0.055 and 0.069 Å in orthorhombic Li_2AuBi and Na_2AuBi. The shortening in d_{Au-Au} has larger magnitude, 0.129 and 0.312 Å, respectively. By contrast, the same volume difference results in a sharp decrease in the dimension of the diamond network – d_{cubic} drops by 1.377 Å from 106.35 to 73.52 Å^3/f.u.

The ΔE terms calculated with VASP are included in Table 4. Again, ΔE_{TOT} matches experimental observations – it is negative for Na_2AuBi (orthorhombic is favored) and positive for Li_2AuBi (cubic is favored) at their experimental volumes. ΔE_{TOT} also reveals that the structural difference between Li_2AuBi and Na_2AuBi is caused by a volume effect. At 73.52 Å^3/f.u., both Li_2AuBi and Na_2AuBi favor the cubic structure; at 106.35 Å^3/f.u., they both prefer the orthorhombic structure.

The ΔICOHP values (Table 5) once again have the same signs with ΔE_{TOT}, indicating that the structural preference can be rationalized through the covalent interactions between Au/Bi atoms. At 106.35 Å^3/f.u., ΔICOHP values are negative for both Li_2AuBi and Na_2AuBi, so the zigzag ribbons provide more stabilization through covalency. The situation is reversede at 73.52 Å^3/f.u. – the diamond network offers more effective covalent interactions between Au/Bi atoms. This is in accordance with the interatomic distances. As mentioned above, from 106.35 to 73.52 Å^3/f.u., the dis-

tances between Au/Bi atoms do not change significantly in the zigzag ribbons, but shrink drastically in the diamond network. So, the latter is expected to experience larger enhancement in covalent interactions upon compression from 106.35 to 73.52 Å^3/f.u. This is, indeed, the case. For instance, in orthorhombic Na_2AuBi, the compression leads to an ICOHP change from –4.52 to –5.62 eV/f.u. – the difference is –1.11 eV/f.u. This is less than in cubic Na_2AuBi, whose ICOHP changes from –4.19 to –6.08 eV/f.u., i.e., by –1.89 eV/f.u. So, as the volume gets smaller, the diamond network becomes increasingly advantageous in covalency.

Although the 3-D diamond network and the 1-D zigzag ribbon are both options for optimized covalent interactions, they offer advantages and disadvantages over each other at different volumes. For the diamond network, symmetry strictly requires that $d_{Au–Bi}$ equals to $(3^{1/2}/4)a$, where a is the lattice parameter of its cubic unit cell, so it is proportional to $V^{1/3}$. $d_{Au–Bi}$ and $d_{Au–Au}$ in the zigzag ribbon do not heavily rely on volume. A change in volume can be absorbed mainly by the separation between the "sheets" containing the zigzag ribbons (lattice parameter a) and/or the separation between zigzag ribbons within one "sheet" (lattice parameter b), while the interatomic distances within the zigzag ribbons do not vary significantly. As a result, at large volume, the zigzag ribbons provide more effective covalent interactions. On the other hand, to assure effective covalent interactions in the diamond network, the volume cannot become too large.

It is not unique to the A_2AuBi systems that a volume increase causes a 3-D network to break down into a lower dimensional structural motif to retain effective covalent interactions. Rather, this effect is frequently observed in many Zintl phases. For instance, NaTl has the diamond Tl network[9] but KTl, with a larger volume,[39] breaks down to separated Tl_6 octahedral clusters. Furthermore, LiSi[40] and LiGe[41] both feature a 3-D network with every Si/Ge atom connected to three other Si/Ge atoms; but in NaSi and NaGe,[42] Si/Ge atoms form isolated Si_4/Ge_4 tetrahedral clusters.

E(*V*) Curves

In all discussions above, the cubic and the orthorhombic structures were always compared at equal volumes per f.u. By doing this, we have successfully identified two factors that affect the relative stability of the zigzag ribbons against the diamond network: (i) the participation of Au 5*d* states in covalent interactions and (ii) the retention of effective covalent interactions by the zigzag ribbons at higher volume. However, in reality, iso-compositional structures do not form at the same volume. For instance, KTl adopts the structure with the Tl_6 octahedron motif[39] at ambient conditions but changes to the double diamond structure at smaller volume achieved by high pressure.[43] Therefore, for each composition discussed above, it is necessary to scan the total energy over a volume range for both the cubic and the orthorhombic structures and compare them at their equilibrium volumes.

The $E(V)$ curves calculated with VASP are shown in Figure 6 and the V_{eq} values obtained from a Murnaghan fitting are listed in Table 6, together the differences in energies and

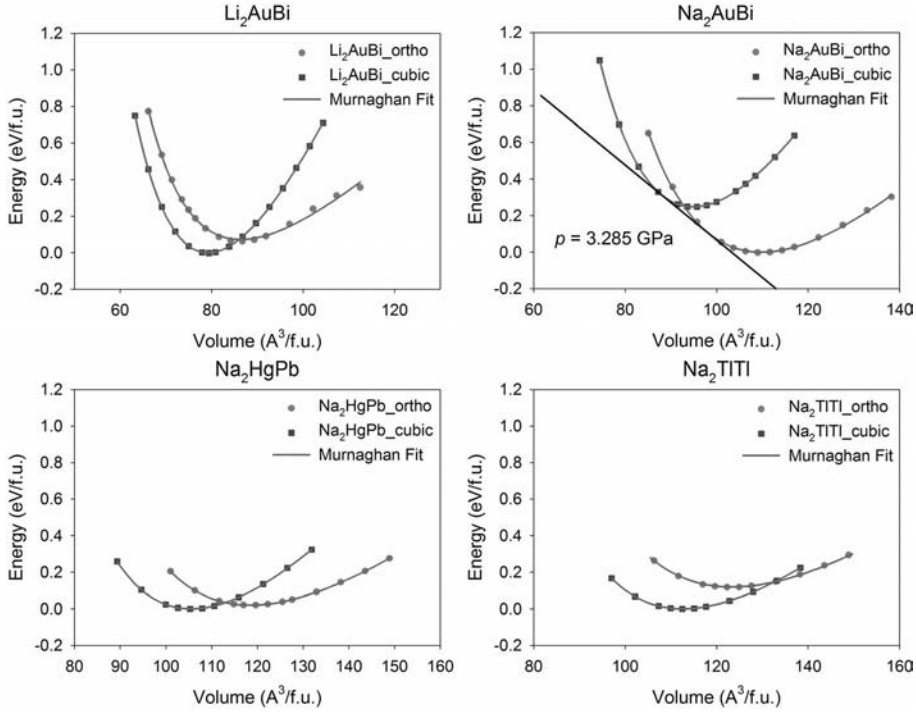

Figure 6. $E(V)$ curves of Li_2AuBi, Na_2AuBi, Na_2HgPb, and Na_2TlTl in both the cubic and the orthorhombic structures calculated with VASP.

Table 6. Equilibrium volumes, differences in energy terms and ICOHP between the orthorhombic and the cubic structures at their equilibrium volumes.

	V_{eq}(ortho) [Å^3/f.u.]	V_{eq}(cubic) [Å^3/f.u.]	ΔE_{ES} [eV/f.u.]	$\Delta E_{electronic}$ [eV/f.u.]	ΔE_{TOT} [eV/f.u.]	ΔICOHP$_{Au/Bi}$ [eV/f.u.]
Li_2AuBi	86.41	79.22	80.0454	–79.98152	0.0639	2.0079
Na_2AuBi	109.82	94.92	187.8556	–188.1054	–0.2498	–0.4306
Na_2HgPb	118.50	105.53	140.8459	–140.8256	0.0203	0.3857
Na_2TlTl	123.39	112.63	82.2605	–82.1438	0.1167	0.8109

ICOHP values between the orthorhombic and the cubic structures at their V_{eq}. The global minimum, which is the lower minimum of the two $E(V)$ curves of each composition and, thus, predicts the structure this composition eventually adopts, occurs for the orthorhombic structure in Na_2AuBi and for the cubic structure in all others, which is in accordance with experiments. But the V_{eq} values of these global minima, which predict the volumes of these compounds, are all higher than the experimental volumes, especially Na_2TlTl, whose predicted 112.63 Å^3/f.u. is more than 9% larger than its experimental 103.22 Å^3/f.u. This overestimation of volume is caused by the PBE pseudopotentials[23] we adopted for VASP calculations and has been observed in other reports.[44,45]

For each composition, V_{eq}(ortho) > V_{eq}(cubic). Also, the cubic structure always offers lower total energy at smaller volume and the orthorhombic always affords lower total energy at larger volume, revealing, once again, that a volume increase shifts favoritism from the diamond network to the zigzag ribbon structural motif. The energy terms exhibit patterns similar to those in Table 4 and Table 5. ΔE_{ES} is always positive, so metallicity favors the cubic structure. $\Delta E_{electronic}$ is always negative, so the localization of valence electrons stabilizes the orthorhombic structure. ΔICOHP always bears the same sign with ΔE_{TOT}, so the covalent interactions between the electronegative atoms determine the relative stability between these two structures – the Zintl–Klemm rationalization is valid here. Therefore, these comparisons made at V_{eq} agree with those made at equal volumes in previous discussions. The $E(V)$ curves also reveal that a pressure induced phase transition can be expected in Na_2AuBi: at pressures exceeding ca. 3.285 GPa, Na_2AuBi is predicted to transform from the orthorhombic into the cubic structure. High pressure synthesis and X-ray crystallography are necessary to test this prediction.

Conclusions

The zigzag ribbon motif in the orthorhombic structure adopted by Na_2AuBi and the diamond network in the cubic structure adopted by Li_2AuBi and Na_2TlTl are both options for optimized covalent interactions between Au/Bi atoms or Tl atoms. The relative stability between these two structures is determined by which structural motif provides more effective covalent interactions. We identified two important factors that can tune the relative stability. The first one is the involvement of 5*d* states in covalent interactions, which stabilizes the zigzag ribbon. The second factor is volume. Due to the symmetry restriction, the diamond network cannot afford effective covalent interactions at high volume and yields to the 1-D zigzag ribbon.

By studying A_2AuBi and comparing the two competing structural motifs, we gained some supplemental conclusions about the Zintl–Klemm concept. Firstly, Zintl phases may consist of elements from not only the *s* and *p* blocks, but also the *d* block in the periodic Table so the structures can be much more complex than what we could expect from those well established electron counting rules, e.g., octet and Wade's rules.[46,47] Secondly, the volume effect is important. Larger "cations," which lead to larger volumes, tend to break down a three-dimensional "anionic" network into a lower-dimensional structural motif, which also provides optimized covalent interactions.

With this and the previous reports,[10] we have demonstrated that by comprehensively considering metallicity, ionicity, and covalency through total energy partitioning, we can effectively rationalize the structures of Zintl phases. There are, of course, many more structural problems within Zintl phases than those addressed in these reports. For instance, some phases with the double diamond structure undergo a tetragonal distortion at low temperature.[48–50] We believe that our methods can be applied effectively to address these problems as well.

Supporting Information (see footnote on the first page of this article): The optimized KTl- and BaCu-type structures, the DOS and COHP curves of LiAl, LiTl, NaTl, and KTl in the seven structure types, the valence electron density maps of CsCl-type LiAl, LiTl, and NaTl, the *sp* projections of the wave functions at Γ- and *L*-points, and the electron density maps of the bands at Γ- and *L*-points.

Acknowledgments

This work was supported by National Science Foundation (NSF) (grant numbers DMR 06-05949 and DMR 10-05765). The computations were done on the CRUNCH system supported by Iowa State University Computation Advisory Committee project 202-17-10-08-0005. We wish to gratefully acknowledge an astute referee, who pointed out the 3-center, 4-electron bonding picture for the $[AuBi]^{2-}$ ribbon.

[1] E. Zintl, W. Dullenkopf, *Z. Phys. Chem. Abt. B* **1932**, *16*, 183.
[2] E. Zintl, G. Brauer, *Z. Phys. Chem. Abt. B* **1933**, *20*, 245.
[3] E. Zintl, *Angew. Chem.* **1939**, *52*, 1.
[4] H. Schäfer, B. Eisenmann, W. Müller, *Angew. Chem. Int. Ed. Engl.* **1973**, *12*, 694.
[5] H. Schäfer, B. Eisenmann, *Rev. Inorg. Chem.* **1981**, *3*, 29.
[6] H. Schäfer, *Ann. Rev. Mater. Sci.* **1985**, *15*, 1.
[7] R. Nesper, *Prog. Solid State Chem.* **1990**, *20*, 1.
[8] *Chemistry, Structure, and Bonding of Zintl Phases and Ions* (Ed.: S. M. Kauzlarich), VCH, Weinheim, Germany, **1996**.

[9] E. Zintl, G. Woltersdorf, *Z. Elektrochem.* **1935**, *41*, 876.
[10] F. Wang, G. J. Miller, submitted to *Inorg. Chem.*
[11] S.-J. Kim, G. J. Miller, J. D. Corbett, *Z. Anorg. Allg. Chem.* **2010**, *636*, 67.
[12] E. M. W. Janssen, J. C. W. Folmer, G. A. Wiegers, *J. Less-Common Met.* **1974**, *38*, 71.
[13] E. M. W. Janssen, G. A. Wiegers, *J. Less-Common Met.* **1978**, *57*, 58.
[14] H. Jagodzinski, *Z. Kristallogr.* **1959**, *112*, 80.
[15] W. P. Davey, *Phys. Rev.* **1923**, *21*, 380.
[16] C. Kolm, S. A. Kulin, B. L. Averbach, *Phys. Rev.* **1957**, *108*, 965.
[17] H. Pauly, A. Weiss, H. Witte, *Z. Metallkde.* **1968**, *59*, 47.
[18] T. A. Albright, J. K. Burdett, M.-H. Whangbo, *Orbital Interactions in Chemistry* Wiley-Interscience, New York, **1985**.
[19] a) G. Kresse, J. Hafner, *Phys. Rev. B* **1993**, *47*, 558; b) G. Kresse, J. Hafner, *Phys. Rev. B* **1994**, *49*, 14251.
[20] G. Kresse, J. Furthmüller, *Comput. Mater. Sci.* **1996**, *6*, 15.
[21] G. Kresse, J. Furthmüller, *Phys. Rev. B* **1996**, *54*, 11169.
[22] G. Kresse, D. Joubert, *Phys. Rev.* **1999**, *59*, 1758.
[23] J. P. Perdew, K. Burke, M. Ernzerhof, *Phys. Rev. Lett.* **1996**, *77*, 3865.
[24] P. Pyykkö, *Chem. Rev.* **1988**, *88*, 563.
[25] G. J. Miller, M. W. Schmidt, F. Wang, T.-S. You, *Structure & Bonding*, Springer, online, DOI: 10.1007/430_2010_24, **2011**.
[26] C. Mues, H. U. Schuster, *Z. Naturforsch. Teil B* **1979**, *34*, 354.
[27] E. Zintl, S. Neumayr, *Z. Phys. Chem. Abt. B* **1933**, *20*, 272.
[28] W. H. Press, B. P. Flannery, S. A. Teukolsky, W. T. Vetterling, in: *Numerical Recipes*, Cambridge University Press, New York, **1986**.
[29] H. J. Monkhorst, J. D. Pack, *Phys. Rev. B* **1976**, *13*, 5188.
[30] B. Eck, *wxDragon 1.4.2*, University of Aachen (RWTH), Germany, **2008**.
[31] F. D. Murnaghan, *Proc. Natl. Acad. Sci. USA* **1944**, *30*, 244.
[32] O. Jepsen, O. K. Andersen, *TB-LMTO 47*, Max-Planck-Institut für Festkörperforschung, Stuttgart, Germany, **2000**.
[33] R. Dronskowski, P. Blöchl, *J. Phys. Chem.* **1993**, *97*, 8617.
[34] U. von Barth, L. Hedin, *J. Phys. C: Solid State Phys.* **1972**, *5*, 1629.
[35] D. Koelling, B. N. Harmon, *J. Phys. C* **1977**, *10*, 3107.
[36] P. P. Ewald, *Ann. Phys. Leipzig* **1921**, *64*, 253–287.
[37] R. G. Pearson, *Inorg. Chem.* **1988**, *27*, 734.
[38] R. Dronskowski, *Computational Chemistry of Solid State Materials*, Wiley-VCH, Weinheim, Germany, **2005**.
[39] Z. Dong, J. D. Corbett, *J. Am. Chem. Soc.* **1993**, *115*, 11299.
[40] J. Evers, G. Oehlinger, G. Sextl, *Angew. Chem.* **1993**, *105*, 1532.
[41] E. Menges, V. Hopf, H. Schaefer, A. Weiss, *Z. Naturforsch. Teil B* **1969**, *24*, 1351.
[42] J. Witte, H. G. von Schnering, *Z. Anorg. Allg. Chem.* **1964**, *327*, 260.
[43] J. Evers, G. Oehlinger, *Phys. Rev. B* **1999**, *59*, 1758–1775.
[44] P. Haas, F. Tran, P. Blaha, K. Schwarz, R. Laskowski, *Phys. Rev. B* **2009**, *80*, 195109.
[45] R. P. Stoffel, C. Wessel, M.-W. Lumey, R. Dronskowski, *Angew. Chem.* **2010**, *122*, 2; *Angew. Chem. Int. Ed.* **2010**, *49*, 2.
[46] K. Wade, *Adv. Inorg. Chem. Radiochem.* **1977**, 18, 1.
[47] D. M. P. Mingos, *Adv. Organomet. Chem.* **1977**, *15*, 1.
[48] H. Ehrenberg, H. Pauly, T. Hansen, J.-C. Jaud, H. Fuess, *J. Solid State Chem.* **2002**, *167*, 1.
[49] H. Ehrenberg, H. Pauly, M. Knapp, J. Gröbner, D. Mirkovic, *J. Solid State Chem.* **2004**, *177*, 227.
[50] M. Gilleßen, R. Dronskowski, *J. Comput. Chem.* **2010**, *31*, 612.

Received: March 25, 2011
Published Online: June 6, 2011

